



1 Sensitivity study of the Regional Climate Model RegCM4 to 2 different convective schemes over West Africa

3

4 Brahim KONE¹, Arona DIEDHIOU^{1,2}, N'datchoh Evelyne TOURÉ¹, Mouhamadou Bamba
5 SYLLA³, Filippo GIORGI⁴, Sandrine ANQUETIN², Adama BAMBA¹, Adama DIAWARA¹,
6 Arsene Toka KOBEA¹

7

8 ¹LAPAMF, Université Félix Houphouët Boigny, Abidjan, Côte d'Ivoire

9 ²Univ. Grenoble Alpes, IRD, CNRS, Grenoble INP, IGE, F-38000 Grenoble, France

10 ³WASCAL Centre of Competence, Ouagadougou, Burkina Faso

11 ⁴International Centre for Theoretical Physics (ICTP), Trieste, Italy

12

13 *Correspondence to:* Arona DIEDHIOU (aronadiedhiou@ird.fr)

14

15 **Abstract.** The latest version of RegCM4 with CLM4.5 as land surface scheme was used to
16 assess the performance and the sensitivity of the simulated West African climate system to
17 different convection schemes. The sensitivity studies were performed over the West Africa
18 domain from November 2002 to December 2004, at spatial resolution of 50km x 50km and
19 involved five (5) convective schemes: (i) Emanuel; (ii) Grell; (iii) Emanuel over land and Grell
20 over ocean (Mix1); (iv) Grell over land and Emanuel over ocean (Mix2); and (v) Tiedtke. All
21 simulations were forced with ERA-Interim data. Validation of surface temperature at 2m and
22 precipitation were conducted using respectively data from the Climate Research Unit (CRU)
23 and Global Precipitation Climatology Project (GPCP) during June to September (rainy season).
24 Quantitative assessment of the sensitivity tests were carried out using the mean bias, the pattern
25 correlation coefficient, the root mean square difference, the probability density function of the
26 temperature bias and the Taylor diagram. Results revealed a better performance of the
27 configuration with Emanuel convection scheme to simulate the spatial and temporal variability
28 of the temperature and the precipitation. Therefore, the configuration of RegCM4 with CLM4.5
29 as land surface model and implementing Emanuel convective scheme is recommended for the
30 study of the West African climate system.

31



32

33 **1 Introduction**

34 Agriculture over West Africa relies mainly on rainfall and is strongly dependent on the West
35 African monsoon. Therefore, the onset, cessation and the amount of expected precipitation
36 associated with the West African Monsoon are of great importance for farmers and accurate
37 simulation and prediction of rainfall and temperature are crucial for various sectors, such as
38 agriculture, energy and health, and for decision-makers. Rainfall over West Africa is strongly
39 related to the meridional migration of the Inter-Tropical zone of convergence (ITCZ) and is
40 modulated by successive active and inactive phases of the monsoon system (Sultan et al., 2003a;
41 Janicot et al., 2011). After a quasi-stationary position around 5° N between mid-April and end
42 of June, the rainfall maxima present an abrupt shift toward the north to hold another quasi-
43 stationary position around 11°N in July-August, bringing precipitation over Central Sahel
44 region (Sultan and Janicot, 2000). This abrupt northward shift is the monsoon ‘‘onset’’ over the
45 Sahel and contrasts with the smooth southward retreat of the ITCZ, followed by the second
46 rainy season over the Guinean Coast in October–November (Sultan et al., 2003b; Janicot et al.,
47 2011). In addition, atmospheric circulations through African Easterly Jet (AEJ), Tropical
48 Easterly Jet (TEJ) and their interaction with convection play an important role in the West
49 African Monsoon (WAM) system (Nicholson 2013) and modulate the summer rainfall (Sylla
50 et al., 2013a). Various climate modeling tools have been applied over West Africa for studying
51 and better understanding of the WAM.

52 General circulation models (GCMs) are unable to include the effects of regional features (Xue
53 et al., 2010) due to their relatively coarse resolution. Regional Climate Models (RCMs) are
54 relevant tools for this purpose since they allow land surface heterogeneity and fine-scale forcing
55 such as complex topography and vegetation variations (Paeth and al., 2006). Moreover,
56 previous studies have shown that they are able to reasonably simulate the WAM climatology
57 (Kamga and Buscarlet, 2006; Sylla et al., 2009) and its variability (Diallo et al., 2012). RCMs
58 contributed to improve our knowledge of the interactions between atmospheric and surface
59 factors affecting the precipitation (Sylla et al., 2011; Browne and Sylla, 2012), of the influence
60 of external forcing such as Sea Surface Temperature (SST, Paeth and A. Hense, 2004), dust
61 (Konare et al., 2008; N'Datchoh et al., 2017) and land-use changes on the dynamic of the
62 monsoon system (Abiodun et al., 2012; Zaroug et al., 2012).

63 RegCM versions (Giorgi et al., 2012; Pal et al., 2007) are the one of the most commonly used
64 among the large range of RCMs to study the climate of West African and of many regions of
65 the world. Compared with the previous version (RegCM3; Pal et al., 2007), the latest release



66 (RegCM4) has been improved with substantial development of the software code and of the
67 physical representations (Giorgi et al., 2012) and with the introduction of CLM (version 3.5
68 and 4.5) as an option to describe land surface processes. Previously it was Biosphere-
69 Atmosphere Transfer Scheme (BATS; Dickinson et al., 1993) only which was used as land
70 surface model. Many studies have shown that the model performs well when using BATS over
71 the West Africa (Sylla et al., 2009; Diallo et al., 2013) but CLM offers improvements in the
72 land-atmosphere exchanges of moisture and energy and in the associated surface climate
73 feedbacks (Steiner et al., 2009). Nonetheless it was shown over India that CLM use may lead
74 to a weaker performance of RegCM than BATS (Halder and al., (2015). Thus, the performance
75 of RegCM4 when using CLM (RegCM4-CLM4.5) needs to be assessed and sensitivities tests
76 have to be conducted on physical processes parameterization to find the optimal configuration
77 of the RCM for a given region and to give the relevant information to RCM users.

78 Among different physical processes in climate models, the convective parameterization is
79 usually considered as the most important when simulating the monsoon rainfall (Im et al., 2008;
80 Leung et al., 2004). Simulations of regional climate are very sensitive to physical
81 parameterization schemes, particularly over the tropics where convection plays a major role in
82 monsoon dynamics (Singh et al., 2011; Srinivas et al., 2013; Gao et al., 2016). One of the main
83 sources of uncertainties in climate prediction is related to the representation of the clouds, which
84 mainly influences the energy response of the models to a disturbance (Soden and Held, 2006;
85 IPCC, 2007). Thus, implementing appropriate convective scheme in dynamic models is needed
86 for realistic simulations.

87 Several sensitivity studies using previous version of RegCM have been conducted over Africa.
88 Meinke et al., (2007) and Djiotang and Kamba (2010) showed that in West Africa, the monsoon
89 precipitations are sensitive to the choice of cumulus parameterization and closure schemes.
90 Brown and Sylla (2012) performed a sensitivity study of RegCM3 to the domain size over West
91 Africa and showed that a large domain is required to capture variability of summer monsoon
92 rainfall and circulation features. Recent study by Adeniyi (2014) using version 4 of RegCM
93 indicated that all convective schemes give good spatial representation of rainfall with biases
94 over West Africa. Komkoura and al., (2016) found that the last release of RegCM implementing
95 Grell as convective scheme with Arakawa-Schubert closure assumption is more suitable to
96 downscale the diurnal cycle of rainfall over Central Africa. However, none of these studies have
97 attempted to investigate a sensitivity study of the Regional Climate Model (RegCM4) to the
98 convective scheme over West Africa with CLM4.5 as the land surface model.



99 This study investigates the performance of RegCM4-CLM4.5 over West Africa using different
100 convection schemes in the aim to identify the “best” configuration option for the region. The
101 paper is structured as follows: the description of the model, data and numerical experiments
102 used to investigate the RegCM4 performance are described in Section 2; Section 3 analyzes and
103 discusses the model’s performance under different convection processes; and the main
104 conclusions are summarized in Section 4.

105

106 **2 Model description, observation datasets and numerical experiments**

107 **2.1 Model description and datasets.**

108 The 4th generation of the ICTP RegCM (hereafter RegCM4) is used in this study. RegCM is a
109 limited-area model using a terrain-following σ -pressure vertical coordinate system and an
110 Arakawa B-grid finite differencing algorithm (Giorgi et al., 2012). The model’s dynamical
111 component is derived from the hydrostatic version of the Pennsylvania State University
112 Mesoscale Model version 5 (MM5; Grell et al., 1994) with improvements on the coupling with
113 an advanced and complex land surface model (CLM3.5 and CLM4.5; Oleson et al., 2008 and
114 2013). In the version used here, the radiation scheme is derived from the NCAR global model
115 CCM3 (Kiehl et al., 1996) and includes representation of aerosols following Solmon et al.,
116 (2006) and Zakey et al., (2006). Turbulent transports of momentum, water vapor and sensible
117 heat in the planetary boundary layer over land and ocean are computed as Holtslag et al., (1990),
118 which allows nonlocal transport in the convective boundary layer. The large-scale precipitation
119 scheme of Pal et al., (2000) referred as SUBgrid EXplicit moisture scheme (SUBEX) includes
120 the subgrid variability in clouds (Sundqvist and al., 1989) and the evaporation and accretion
121 processes for stable precipitation. Ocean surfaces fluxes of momentum, heat and moisture are
122 represented using the scheme of Zeng and al., (1998) with a drag coefficient-based bulk
123 aerodynamic procedure and considering the influence of surface friction velocity on roughness
124 length computed following Smith (1988) and Brutsaert (1982), respectively for momentum and
125 heat (and also moisture).

126 The soil-vegetation-atmosphere interaction processes are parameterized using Community
127 Land Model (CLM version 4.5; Oleson et al., 2013). CLM4.5 presents in each grid cell the
128 possibility to have fifteen soil layers, up to five snow layers, five different land unit types and
129 sixteen different plant functional types (Lawrence et al., 2011; Wang et al., 2016). RegCM4-
130 CLM4.5 proposes five different convective schemes (Im et al., 2008); Giorgi et al., 2012): the
131 modified-Kuo scheme (Anthes et al., 1987), the Tiedtke scheme (Tiedtke 1989), the Emanuel
132 scheme (Emanuel 1991), the Grell scheme (Grell 1993) and the Kain-Fritsch scheme (Kain-



133 Fritsch, 1990; Kain 2004) with the possibility to combine different schemes over ocean and
134 land (called as ‘mixed’ convection).

135 For this sensitivity study, the model was run at its standard configuration with 18 vertical sigma
136 layers (model top at 50 hPa) and with initial and boundary conditions provided by the European
137 Centre for Medium Range Weather Forecasts reanalysis ERA-interim (Simmons et al., 2007;
138 Uppala et al., 2008) at an horizontal resolution of 50 km and a temporal resolution of 6 hours
139 (00:00, 06:00, 12:00 and 18:00 UTC). Sea-surface temperatures (SST) were from NOAA
140 optimal interpolation weekly SST data (Reynolds et al., 2007). The terrain characteristics
141 (topography and land use data) were derived from United States Geological Survey (USGS)
142 and Global Land Cover Characterization (GLCC; Loveland et al., 2000) respectively at 10 min
143 horizontal resolution.

144 We focus our analysis on the precipitation and on the air temperature at 2m in the summer of
145 June-July-August-September (JJAS) over mainland West Africa. To reduce uncertainty due to
146 lack of surface climate observations over the region (Nikulin et al., 2012; Sylla et al., 2013a),
147 the simulated precipitation is validated using two observational datasets including the monthly
148 mean precipitation at 2.5° horizontal resolution from Global Precipitation Climatology Project
149 (GPCP; Adler et al., 2003) available from 1979 to present and the 0.25° high resolution dataset
150 of Tropical Rainfall Measuring Mission 3B43V7 (TRMM) available from 1998 to 2013
151 (Huffman et al. 2007). The simulated 2m temperature is validated using also two observational
152 datasets including the Climate Research Unit (CRU) time series version 3.20 gridded at 0.5°
153 horizontal resolution from the University of East Anglia and available respectively from 1901
154 to 2011 (Harris et al., 2013), and the University of Delaware version 3.01 (UDEL) gridded
155 dataset at 0.5° horizontal resolution available from 1900 to 2010 (Legates and Willmott, 1990).
156 The simulated atmospheric fields are compared with ERA-Interim reanalysis available from
157 1979 to present at 1.5° horizontal resolution (Dee et al., 2011). All products are remapped onto
158 the RegCM4 grid (0.44°×0.44°) using a bilinear interpolation method to facilitate the
159 comparison (Nikulin et al., 2012). The model’s performance is further examined in four sub-
160 regions (Fig. 1), each with different characteristics of the annual cycle of rainfall: Central Sahel
161 (10°W–10°E; 10°N–16°N), West Sahel (18°W–10°W; 10°N–16°N), Guinea Coast (15°W–
162 10°E; 3°N–10°N) and West Africa (20°W–20°E; 5°S–21°N).

163

164 **2.2 Convective schemes**

165 The convective precipitation parameterizations used in this study are Tiedke (1989), Emanuel
166 (1991) and Grell (1993) schemes.



167 The Emanuel (1991) scheme assumes that the mixing in clouds is highly episodic and
168 inhomogeneous (in contrary to a continuous entraining plume) and takes into account
169 convective fluxes based on an idealized model of sub-cloud-scale updrafts and downdrafts.
170 Convection is triggered when the level of neutral buoyancy is greater than the cloud base level.
171 Between these two levels, air is lifted and a fraction of the condensed moisture forms
172 precipitation while the remaining fraction forms the cloud. The cloud is supposed to mix with
173 the air from the environment according to a uniform spectrum of mixtures that ascend or
174 descend to their respective levels of neutral buoyancy. The mixing entrainment and detrainment
175 rates depend on the vertical gradients of buoyancy in clouds. Emanuel scheme includes a
176 formulation of the auto-conversion of cloud water into precipitation inside cumulus clouds.
177 In the Grell (1993) scheme, deep convective clouds are represented by an updraft and a
178 downdraft that are undiluted and mix with environmental air only in cloud base and top. Heating
179 and moistening profiles are derived from latent heat released or absorbed, linked with the
180 updraft-downdraft fluxes and compensating motion (Martinez-Castro et al., 2006). Two types
181 of Grell scheme convective closure assumption can be found in RegCM4. In the Arakawa–
182 Schubert (1974) closure (AS), a quasi-equilibrium condition is assumed between the generation
183 of instability by grid-scale processes and the dissipation of instability by sub-grid (convective)
184 processes. In the Fritsch–Chappell (FC) closure (Fritsch and Chappell, 1980), the available
185 buoyant energy is dissipated during a specified convective time period (between 30 min and 1
186 hour).
187 Similarly, the Tiedtke (1989) scheme is a mass flux convection scheme, albeit it considers a
188 number of cloud types as well as cumulus downdrafts that can represent deep, mid-level and
189 shallow convection (Singh et al., 2011; Bhatla et al., 2016). The closure assumptions for the
190 deep and mid-level convection are maintained by large-scale moisture convergence, while the
191 shallow convection is sustained by the supply of moisture derived from surface evaporation.

192

193 **2.3 Numerical experiments and methodology**

194 Five experiments using the convection schemes of (1) Emanuel over land and Grell over ocean
195 (mix1), (2) Emanuel, (3) Grell, (4) Tiedtke and (5) Grell over land and Emanuel over ocean
196 (mix2) are conducted using RegCM4-CLM4.5 with 18 sigma levels at 50 Km horizontal
197 resolution for the period from November 2002 to September 2004. The two first months (i.e.
198 November and December 2002) was considered as spin-up time and not included in the
199 analysis. The analyses will focus on the rainy season from June to September (JJAS). As
200 quantitative measurements of model skills, we consider mean bias (MB) which is the difference



201 between the area-averaged value of the simulation and the observation, the spatial root mean
202 square difference (RMSD) and the spatial correlation called Pattern Correlation Coefficient
203 (PCC) and the distribution of Probability Density Function (PDF) of the temperature bias. The
204 RMSD, PCC and the PDF provide information at the grid-point level while the MB does so at
205 the regional level. A Taylor diagram (Taylor, 2001) is used to summarize assessments above
206 and to show the deviation of different model configurations results from observations.

207 As assumed in Gao et al., (2016), the temperature bias in JJAS present a normal mode type of
208 distribution. The PDF is expressed as:

$$209 \quad \frac{1}{\sigma\sqrt{2\pi}} e^{-\frac{(x-\mu)^2}{(2\sigma)^2}}$$

210 Where μ is the mean and σ the standard deviation of temperature bias.

211 The PDF is characterized by its bell shaped curve, the temperature biases distribute
212 symmetrically around the mean bias temperature value in decreasing numbers as one moves
213 away from the mean. The empirical rule states that for a normal distribution, nearly all of the
214 data will fall within three standard deviations of the mean. The empirical rule can be broken
215 down into three parts:

- 216 • 68% of grid points fall within the first standard deviation from the mean.
- 217 • 95% of grid points fall within two standard deviations from the mean.
- 218 • 99.7% of grid points fall within three standard deviations from the mean.

219 The rule is also called the 68-95-99.7 Rule or the Three Sigma Rule. Thus, they constitute
220 measurements of model performance and systematic model errors. These metrics are computed
221 for each of the sub-regions indicated in Figure 1.

222

223 **3 Results and discussion**

224 **3.1 Temperature**

225 The spatial distribution of averaged temperature during JJAS over 2003-2004 from CRU and
226 UDEL observations (resp. Fig. 2a, b) is compared to the temperature simulated by RegCM4
227 using the convection schemes: Mix1, Emanuel, Grell, Tiedtke and Mix2 (resp. Fig. 2c-g).
228 Figure 3 shows the associated mean model biases relatively to CRU for observation (UDEL;
229 Fig.3a) and the model simulations (Fig. 3b-f). Table 1 reports the PCC and the RMSD between
230 the simulated and observed temperature calculated for Guinea Coast, Central Sahel, West Sahel
231 and the entire West Africa domain. The CRU temperatures presents a zonal distribution in West
232 Africa with maximum ($>34^{\circ}\text{C}$) in the Sahara and lowest temperatures ($<22^{\circ}\text{C}$) over the Guinea
233 Coast and over complex terrains such as the Jos plateau, Cameroon mountains and Guinean



234 highlands. The UDEL observation (Fig. 2b) shows similarity with CRU in terms of spatial
235 distribution with PCC larger than 0.98 over the entire West African domain (see Table 1).
236 However, UDEL depicts a sparse distribution with a mixture of warm and cold bias over the
237 Sahara and along of Nigeria/Cameroon border around $\pm 2^{\circ}\text{C}$ (see Fig. 3a). There is also a good
238 agreement between model simulated temperatures and CRU observation with the PCCs more
239 than 0.93 (Table 1) over West Africa. All model configurations well reproduce the general
240 features of the observed pattern including the meridional surface temperature gradient zone
241 between Guinea Coast and the Saharan desert. This temperature gradient is important for the
242 evolution of the African Easterly Jet (AEJ) (Cook 1999; Thorncroft and Blackburn, 1999). All
243 model configurations (Fig. 3b-d, f) exhibit a similar dominant cold biases except the Tiedtke
244 configuration (Fig. 3e) in the Sahara desert at the central part of Mauritania and Niger, and
245 along the Guinea Coast region. The greater cold bias with value up to -5°C occurs when using
246 Grell configuration while, simulation using Tiedtke configuration depicts a dominant warm bias
247 up to 4°C mainly located in Central Sahel around 12°N (Fig. 3e). One effect of the warm bias
248 shown in Tiedtke simulation is to shift the zone of meridional temperature gradient southward
249 relative to its observed position (Fig. 2f). However, it is difficult to determine the origin of
250 RCM temperature biases as they involve changes in surface-atmosphere interactions and as they
251 are function of many factors such as surface albedo, cloudiness, temperature advection and
252 surface water and energy fluxes (Tadross et al., 2006; Sylla et al., 2012).

253 For a quantitative evaluation of the performance of these sensitivity tests, the PDF statistical
254 tool was used. The PDF distributions of the temperature bias in JJAS is shown in Figure 4 for
255 Guinea Coast, Central Sahel, West Sahel and the entire West Africa domain. The PDF
256 distribution shows a general dominant cold bias (see Fig. 4a-d) in model simulations over most
257 of study domain, except with Tiedtke configuration in the Central Sahel region.

258 Over Guinea Coast region, Grell configuration presents a colder bias (reached -6°C) compared
259 to the other configurations. However, Emanuel simulation shows the lower RMSD about
260 1.29°C with a PCC larger than 0.77 (see Table 1). For Central Sahel region (Fig. 4b) a warmer
261 bias is found in Tiedtke simulation, while a colder bias is found in Grell and Mix2
262 configurations (see Fig. 4b). Emanuel configuration shows a lower value of RMSD about
263 0.67°C and a higher PCC larger than 0.95 compared to the other model simulated temperatures
264 (see table 1). In West Sahel a colder bias is found with Grell scheme (see Fig. 4c) while
265 Emmanuel and Tiedtke simulations show a mixture of cold and warm bias. Configuration of
266 RegCM with Emanuel presents a better performance with a lower RMSD and higher PCC
267 values compared to the other simulations in West Sahel. Over the entire West Africa domain



268 (see Fig.4d), Grell and Tiedtke present respectively a colder and warmer bias. Generally, with
269 respect to temperature simulations, a better performance of RegCM4 is obtained when using
270 Emmanuel scheme.

271

272 3.2 Precipitation

273 The spatial distribution of mean JJAS precipitation (2003–2004) over West Africa is shown in
274 Figure 5 for observations GPCP and TRMM (resp. Fig. 5 a-b) and for RegCM4 simulations
275 with the following convective schemes Mix1, Emmanuel, Grell, Tiedtke and Mix2 (resp. Fig.5
276 c-g). Sylla et al. (2013a) argued that over Africa, GPCP is more consistent with gauge based
277 observations, whilst Nikulin et al. (2012) found a significant dry bias over tropical Africa in
278 TRMM compared to GPCP. We therefore select, for precipitation, GPCP as our main
279 observational reference in this paper.

280

281 Figure 6 shows the corresponding precipitation mean biases relatively to GPCP for TRMM (Fig
282 6a) and for the different simulations configurations (Mix1, Emmanuel, Grell, Tiedtke and Mix2;
283 Fig 6b-f respectively). GPCP depicts a zonal band of rainfall decreasing from North to South.
284 Precipitation maxima are found in orographic regions of Guinea highlands, Jos Plateau, and
285 Cameroon Mountains. Differences between TRMM and GPCP observation products (Table 2)
286 can reach up to -5.26% at sub-regional levels, while over the entire West Africa it does not
287 exceed 0.82%. Although both observation products exhibit some differences (Fig.6a-c), their
288 patterns show a good agreement, with PCCs more than 0.96 over the entire West Africa domain
289 (Table 2). TRMM underestimates the rainfall intensity over Guinea Coast and Central Sahel
290 regions (respectively no more than -0.86% and -5.12%) and overestimates the rainfall intensity
291 over West Sahel and the entire West Africa domain reaching respectively 3.48% and 0.83%.
292 The spatial distribution of rainfall is well reproduced by all model configurations with PCCs
293 values within the range 0.61 and 0.89 over the entire West African domain. The dominant
294 feature in these simulations is the dry bias over West Africa domain (Fig. 6b-f), which is more
295 pronounced in the Tiedtke configuration (see Table 2). The warmer bias over Central Sahel in
296 Tiedtke configuration (Fig.3e) is consistent with the drier bias found in the same region (see
297 Table 2 and Fig.6e), as less rainfall would induce less evaporative cooling and increase the
298 insolation through decreased cloud cover. However, the Table 2 reveals that Mix1 and Emanuel
299 show a better performance with a lower mean biases and greater PCC compared to the others
300 model simulations over the entire West African domain and its sub-regions.

301



302 In order to understand the origins of the model rainfall biases, we analyzed the JJAS midlevel
303 (850–300 hPa) vertically integrated water vapor mixing ratio and the 650 hPa low-level wind
304 (African Easterly jet, AEJ) over West Africa averaged over the 2003–2004 period (Fig. 7). The
305 AEJ is the most prominent feature affecting the West African Monsoon through its role in
306 organizing convection and precipitation over the region (Cook 1999; Diedhiou et al., 1999;
307 Mohr and Thorncroft, 2006; Sylla et al., 2011). Areas with larger water vapor mixing ratio
308 corresponds to the areas of maximum precipitation in observations (see Fig. 5a-b). Around 9°N
309 the weaker easterly wind (AEJ) contributes to enhance the moisture convergence which results
310 in an increase of water vapor and precipitation (see Fig. 5a-b). All model configurations show
311 some quantitative differences compared to ERA-Interim in both the wind flux and the water
312 vapor mixing ratio.

313 The underestimation of vertically integrated water vapor mixing ratio is larger in Grell and
314 Mix2 simulations (Fig. 7 c, e) over the Guinea Coast and Atlantic Ocean compared to those of
315 Mix1, Emanuel and Tiedtke (Fig. 7 a, b, e). Mix1 and Emanuel configurations reproduce better
316 the spatial extent of the moisture convergence than the others model configurations (Fig.7b, c).
317 All model configurations simulate a stronger easterly wind flux (AEJ) than observed in
318 particular over the Guinea Coast and Atlantic Ocean inducing a negative impact on simulated
319 precipitations in the sub-regions (see Fig. 5c–g). Another possible explanation of model
320 rainfall biases is further discussed in Brown and Sylla (2011) whereby a sensitivity study on
321 the domain size with RegCM3 over West Africa showed that RegCM3 simulates drier
322 conditions over a default domain (RegCM-D1) quite similar to our domain size used in this
323 study.

324 A Taylor diagram is used to give a combined synthesized view of the pattern correlation
325 coefficient and the JJAS standard deviation of precipitation from the different sensitivity studies
326 with respect to GPCP over Guinea Coast, Central Sahel, West Sahel and West Africa. Model
327 standard deviations are normalized by the observed value from GPCP (indicated by REF, see
328 Fig.8). For the entire West Africa domain, the diagram shows Tiedtke and Emanuel outperform
329 the others configurations with values of standard deviation normalized much closer to 1.
330 However Emanuel configuration present a better spatial correlation reaching 0.8 as compared
331 to Tiedtke configuration. Over Guinea Coast sub-region Grell and Emanuel present better values
332 of standard deviation normalized. However, in regarding the spatial correlation value about 0.7
333 Emanuel configuration is the best. For West and Central Sahel, Mix1 and Emanuel are closer
334 to observation. However, Emanuel outperforms Mix1 configuration with a good spatial
335 correlations scores between 0.7 and 0.8 respectively over Central and West Sahel sub-regions.



336 From the Taylor diagram, it can be inferred that Emanuel performs better regarding the standard
337 deviation normalized and the pattern correlation over the entire West African domain and its
338 sub-regions.

339 Based on previous experience and studies, Gao and al., (2016) noted that use of the Emanuel
340 convection scheme in RegCM3 and RegCM4 over China tends to simulate too much
341 precipitation when using BATS as the land surface scheme. They explained that it is mainly
342 due to the fact that the Emanuel scheme responds quite strongly to heating from the surface
343 land as compared to Grell and Tiedtke convection schemes, once convection is triggered. BATS
344 with only two soils levels depth maximizes this response; this is why Emmanuel is too wet
345 when using BATS as compared to Grell and Tiedtke. By contrast, CLM uses several soil layers
346 down to a depth of several meters; therefore, the upper soil temperatures respond less strongly
347 to the solar heating. Precipitation amount is much reduced when using CLM, which is good for
348 Emanuel but not good for Grell and Tiedtke (Gao and al., 2016) while the combination of BATS
349 with Grell and Tiedtke shows good performance (Gao et al., 2012; Ali et al., 2015).

350 In conclusion, although RegCM4-CLM4.5 shows some weaknesses, such as a dry bias over
351 most of Central Sahel and Guinea Coast region, its performance in replicating the spatial
352 distribution of rainfall appears in line with that documented in previous studies using the
353 previous version RegCM3 (Sylla et al. 2009; Abiodun et al.2012).

354

355 **3.3 Mean annual cycle**

356 In this section, we examine the effect of the convection scheme in the characterization of the
357 three distinct phases of the West African Monsoon: the onset, the high rain period and the
358 southward retreat of the monsoon rain band (Sultan et al., 2003). Such behavior is best
359 represented by a meridional cross-section (time-latitude Hovmoller diagram). This diagram
360 provides a robust framework to assess RCM's skills in simulating seasonal and intraseasonal
361 variations of the WAM, and thus the mechanisms of the region's rainfall (Hourdin et al., 2010).
362 Figure 9 shows the time-latitude diagrams of rainfall averaged over the region between 10°E
363 and 10°W for observations GPCP and TRMM (resp. Fig 9a-b) and for model simulations using
364 Mix1, Emmanuel, Grell, Tiedtke and Mix2 convection schemes (resp. Fig 9c-g). The averages
365 are taken for the period 2003–2004 and displayed throughout the year. This figure shows that
366 the three distinctively of monsoon phases are well represented by TRMM than GPCP (resp.
367 Fig.9a, b). TRMM observation shows a first rainy season from mid-March up to mid-June over
368 the Gulf of Guinea and Guinea Coast with a northward extension of the rain belt up to about
369 5°N (Fig.9b). The monsoon jump is characterized by a sudden cessation of precipitation



370 intensities (Sultan and Janicot, 2000, 2003) and occurs from mid-June to early July, when the
371 rain band core moves suddenly northward to about 10°N (Fig.9b). This indicates the beginning
372 of the rainy season over the Sahel with a peak reached in August between 9° and 12°N over
373 Central Sahel. A gradual retreat of the monsoon starts in end of August and it is well shown by
374 GPCP (Fig.9a), with a decrease in intensity and a southward migration of the rain band. There
375 are both similarities and differences across the two observation datasets TRMM and GPCP.
376 Both datasets agree in area of rainfall maximum intensity around 4°N despite a more intense
377 peak of rainfall for TRMM compare to GPCP (resp. Fig.9a, b). The monsoon jump
378 characterized by a discontinuity sharp is not well defined in GPCP compared to TRMM. In
379 addition, GPCP shows wet conditions during the retreat phase in July to September compared
380 to TRMM (Fig.9a, b).

381 Mix1, Emanuel, and Grell model configurations (resp. Fig.9c-e) capture the three phases of the
382 seasonal evolution of the WAM, while Tiedke and Mix2 simulations fail to reproduce them in
383 particular the rainy season over Central Sahel. However Emanuel and Mix model
384 configurations (resp. Fig. 6c, d) overestimate rainfall amounts during the two rainy seasons over
385 Guinea Coast, mostly as a result of an overestimate of the precipitation over the orographic
386 regions of Guinea highlands, Jos Plateau, and Cameroon Mountains. Mix1 and Mix2
387 configurations are respectively wetter and drier compared to the others model configurations
388 (resp. Fig. 9c, g). Generally, the three monsoon phases are well shown by Grell simulation,
389 albeit it is drier compared to the others model simulations.

390 Another analysis of the annual cycle consists of considering the area-averaged (land-only grid
391 points) value of monthly rainfall and temperature over the Gulf of Guinea, the Central Sahel
392 and the entire West African domain (Figures 10 and 11). This allows better identification of
393 rainfall and temperature minima and peaks. Figure 10a-d shows respectively the annual cycle
394 of precipitation averaged over Guinea Coast, Central Sahel, West Sahel and the entire West
395 African domain. Over the Guinea Coast (Fig 10a), both GPCP and TRMM observations show
396 a primary maximum in June and a secondary one in September. The Mix1 and Tiedtke model
397 configurations simulate an early first peak in May while Emanuel, Grell and Mix2
398 configurations well capture the observed peak in June. We note that model configurations well
399 reproduce the timing of the mid-summer break and second rainfall peak in September but they
400 underestimate its magnitude, although Mix1 simulation result is higher and much closer to
401 observations compared to the others model simulations.

402 In both Central Sahel and West Sahel, observations (GPCP and TRMM) display a dry spring
403 (from January to March) and winter (from October to December) and a wet summer (from June



404 to September) with a well-defined peak occurring in August. Model configurations reproduce
405 both phase of the annual cycle and the observed rainfall peak in August except Emanuel
406 configuration which shifts it in September over West Sahel region. Model simulations
407 underestimate the peak intensity compare to observations. However Mix1 configuration rainfall
408 peak is much closer to observation for both Central Sahel and West Sahel regions (resp. Fig
409 10b, d) compared to the others model simulations. Over the entire West African domain, the
410 annual cycle (Fig 10c) is smoother with a notable shift of the peak in September in the different
411 model configurations. All the model configurations underestimate the rainfall peak and shift it
412 in October. However, Mix1 and Emanuel model simulations are much closer to observed annual
413 cycle of precipitation compared to the others. In resume Mix1 simulation compared to the others
414 better reproduce the observed annual cycle of precipitation over the sub-regions and the entire
415 West African domain.

416 The annual cycles of temperature for Central Sahel, West Sahel and the entire West African
417 domain of Mix1, Emmanuel, Grell, Tiedtke and Mix2 convection schemes are shown in Figure
418 11b-d. The observations (CRU and UDEL) indicate a cooler winter from December to February
419 and warmer pre and post-monsoon periods with relative minima occurring during August.
420 While over Guinea Coast, both winter and post monsoon are cooler and only the pre monsoon
421 phase is warmer (Fig. 11a). Models configurations present similar seasonal variation of the
422 mean monthly temperature at 2 m compared to observations, but do exhibit some differences.

423 Over Guinea Coast model simulations underestimate the magnitude of the temperature
424 compared to observations. However, Tiedtke configuration is higher and much closer to
425 observations compared to the others model simulations throughout the year (Fig.11a). Over
426 Central Sahel region, Grell and Tiedtke capture well the seasonal variation from November to
427 June in particular the first peak in August compared to the others models simulations. During
428 the summer (JJAS) Emanuel and Mix1 quite well reproduce the observed precipitation annual
429 cycle (Fig.11b). Therefore, model simulations underestimate the seasonal variation of
430 temperature over the entire West African domain. Although Tiedtke simulation overestimates
431 the mid-summer break period, it is much closer to observed annual cycle of temperature
432 throughout the year compared to the others model simulations. Over the West Sahel, model
433 simulations quite well reproduce the annual cycle of temperature except Grell and Mix2
434 configurations in particular during the summer (JJAS). In summary Tiedtke simulation better
435 reproduce the observed annual cycle of temperature throughout the year over the sub-regions
436 and the entire West African domain compared to the others model configurations.



437 The divergences in the RCMs annual cycles arise mostly from their different abilities to
438 simulate the main features responsible of triggering and maintaining the WAM precipitation
439 (Gbobaniyi E. et al., 2013). Among them, we have the monsoon flow, the African Easterly Jet
440 (AEJ), the Tropical Easterly Jet (TEJ) and the Africa Easterly Waves (AEWs) (Diedhiou et al.,
441 1999; Sylla et al., 2013b). .

442

443 **3.4 Wind profile**

444 The atmospheric circulations and their interactions with ITCZ play an important role in the
445 WAM system (Nicholson 2013). Thus, this section aims to analyze the impact of the choice of
446 convection scheme in the simulations of zonal winds features, including the near-surface
447 westerly component (the West African Monsoon, WAM), the African Easterly Jet (AEJ) and
448 the Tropical Easterly Jet (TEJ) in the mid and upper troposphere respectively. Figure 12 depicts
449 the vertical cross section of the JJAS mean of the zonal wind averaged between 10°W and 10°E
450 for ERA-Interim (Fig.12a) and model configurations in Mix1, Emmanuel, Grell, Tiedtke and
451 Mix2 convection schemes (resp. Fig.12 b-f). The reanalyse ERA-Interim (Fig. 12a) displays
452 the monsoon flow winds below 800 hPa at 2-18°N with two cores merged over both Guinea
453 Coast (centered at 6°N) and Central Sahel (centered at 15°N) sub-regions, the AEJ in the mid-
454 levels centered at 12°N and the TEJ in the upper tropospheric levels at 200 hPa centered at 5°N
455 (Fig12 a). All model configurations well reproduce the zonal wind features despite some biases.
456 Model simulations Mix1, Emanuel, Grell and Tiedtke present a strong core of monsoon flow
457 compared to Era-Interim (reaching 6m/s). The stronger and weaker monsoon flows are found
458 with Mix1 and Mix2 configurations respectively compared to the others configurations.
459 However, model simulations well reproduce the limit of the surface westerly flow compared to
460 its position. Of particular interest is the core of the AEJ in the mid-tropospheric levels, which
461 is greatly weakened with Mx1 and Emanuel. While AEJ magnitude core is well defined in Grell
462 and Mix2 simulations at 12°N, but its spatial extent is somewhat reduced. This location of the
463 AEJ in Grell and Mix2 simulation is consistent with the location of the region of zonal
464 temperature gradient (see resp. Fig. 3e, g), as the AEJ is associated with the surface temperature
465 gradient (Cook 1999; Thorncroft and Blackburn 1999). While Tiedtke simulation shifts the
466 location of AEJ core at 8°N in agreement with the warm bias shown in Tiedtke configuration
467 (see Fig.4e). The TEJ at 200 hPa and 5°N is very similar in model simulations compared to the
468 ERA-Interim reanalysis. However, the core of the jet is weaker in Tiedtke configuration
469 compared to the others model simulations. An overall, Grell configuration outperforms
470 simulations of the main features of the zonal wind compared to the others model simulations.



471

472 **4 Summary and conclusion**

473 The latest released RegCM4 have been performed over West Africa for two years (2002-2003)
474 to assess its performance using five convective parameterizations: (a) the Emanuel scheme, (b)
475 Emanuel over land and Grell over Ocean (Mix1), (c) the Grell scheme, (d) the Tiedke scheme
476 and (e) Grell over land and Emanuel over Ocean scheme (Mix2). The sensitivity of the model
477 to different convection schemes were validated using observations. The main findings and
478 conclusions can be summarized as follows:

- 479 (1) Compared with the previous version of RegCM, RegCM4-CLM also shows a general
480 cold bias over West Africa. However in Central Sahel region, Tiedtke simulation
481 presents a warm bias. This warm bias tends to displace the meridional temperature
482 gradient southward relative to its observed position. An overall, with respect to
483 temperature, better performance are obtained when using Emanuel scheme.
- 484 (2) With respect to the precipitation, the dominant feature in model simulations is a dry bias
485 which is more pronounced when using Tiedtke convection scheme. Considering the
486 good performance over the entire West Africa domain and its sub-regions in the
487 temperature and precipitation simulations, we suggest Emanuel convection scheme
488 when using RegCM4-CLM4.5 over West Africa.
- 489 (3) Simulations when using Mix1 and Emanuel schemes well reproduce the spatial extent
490 of moisture convergence of the ERA-Interim reanalyses compared to the others
491 convection schemes. However, in the mid-levels of the atmosphere, model simulations
492 show an easterly wind flux (AEJ) stronger than observed in particular over the Guinea
493 Coast and Ocean Atlantic below the latitude 4°N, creating an increased subsidence and
494 has a negative effect on simulated precipitations there. This is a possible explanation of
495 a dry bias over West Africa domain. However, the vertical features of the zonal wind,
496 including the near-surface westerly component, the AEJ and the TEJ in the mid and
497 upper troposphere are better simulated when using Grell convection scheme compared
498 to the others model simulations
- 499 (4) The time evolution of simulation when using Grell convection scheme rainfall matches
500 well with the observed evolution, including the timing of the discontinuous northward
501 jump of the main rainfall band in late June, albeit it is drier compared to Mix1 and
502 Emanuel convection scheme.
- 503 (5) Over Central Sahel and West Sahel, the mean annual cycle of precipitation and
504 temperature, with the single peaked rainy season is especially well captured in terms of



505 timing despite the fact that all model simulations underestimated the magnitude.
506 However, simulations using Mix1 reproduce better the annual cycle of precipitation
507 compared to the others schemes.

508 (6) Over Guinea Coast, Mix1 and Tiedtke model simulations failed to reproduce the double
509 peaks rainy seasons, while Emanuel, Grell and Mix2 simulations well reproduce them
510 but underestimate their amplitude. The bimodal nature of rainfall associated with the
511 Guinea sub-region is not so well defined when averaging rainfall over the entire West
512 African domain. This emphasizes the importance of separating regions into
513 homogeneous precipitation sub-regions for evaluation analyses.

514 (7) The mean annual cycle of temperature, is well reproduce in simulation when using
515 Tiedtke convection scheme throughout the year over the sub-regions and the entire West
516 Africa domain compared to the others model simulations.

517
518 As more advanced package compared to the previously version of RegCM with BATS,
519 CLM4.5 can be considered as the primary land surface processes option in RegCM4.
520 Therein, the use of Emanuel scheme is recommended over the West African region. We
521 plan to use this configuration in long-term, multi-decadal simulations, to further evaluate
522 the model capability in reproducing the mean climatology, as well as the variability of
523 climate extremes over the region.

524

525 **Acknowledgements**

526 This work is dedicated to the memory of Prof Abdourahamane Konaré with whom we
527 started this assessment. The authors thank the Institute of Research for Development (IRD,
528 France) and Institute of Geosciences for Environment (IGE, University Grenoble Alpes) for
529 providing the facility (the Regional Climate Modelling Platform) to perform these
530 simulations and the IT support funded by IRD/PRPT contract at the University Felix
531 Houphouet Boigny (Abidjan, Côte d'Ivoire). The authors are grateful to all students,
532 technicians, engineers and researchers involved at ICTP (Abdus Salam International Centre
533 of Theoretical Physics; Trieste, Italy) on the development and the improvement of the
534 regional climate model RegCM.

535



536 **References**

- 537 Abiodun BJ, Adeyewa ZD, Oguntunde PG, Salami AT, Ajayi VO. 2012. Modeling the impacts
538 of reforestation on future climate in
539 West Africa. *Theor. Appl. Climatol.* 110(1–2): 77–96.
540
- 541 Adeniyi MO. 2014. Sensitivity of different convective schemes in RegCM4.0 for simulation of
542 precipitation during the Septembers of 1989 to 1998 over West Africa. *Theor. Appl. Climatol.*
543 115(1–2): 305–322, doi: 10.1007/s00704-013-0881-5.
544
- 545 Adler RF et al (2003). The version-2 Global Precipitation Climatology Project (GPCP) monthly
546 precipitation analysis (1979–present). *J Hydrometeorol* 4(6):1147–1167
547
- 548 Ali S., L. Dan, C. B. Fu, and Y. Yang, 2015: Performance of convective parameterization
549 schemes in Asia using RegCM: Simulations in three typical regions for the period 1998–2002.
550 *Adv. Atmos. Sci.*, 32(5), 715–730, doi:10.1007/s00376-014-4158-4.h
551
- 552 Arakawa A, Schubert WH (1974) Interaction of a cumulus cloud ensemble with the large scale
553 environment. Part I. *J Atmos Sci* 31: 674–701
554
- 555 Bhatla R., S. Ghosh, B. Mandal, R.K. Mall, Kuldeep Sharma. "Simulation of Indian summer
556 monsoon onset with different parameterization convection schemes of RegCM-4.3",
557 *Atmospheric Research*, 2016. DOI : 10.1016/j.atmosres.2016.02.010
558
- 559 Browne N.A.K., Sylla MB. 2012. Regional climate model sensitivity to domain size for the
560 simulation of the West African monsoon rainfall. *Int. J. Geophys.* Article ID 625831, DOI:
561 10.1155/2012/625831.
562
- 563 Brutsaert W (1982) *Evaporation into the atmosphere: theory, history and applications*. USA:
564 Reidel Hingham Mass, 299 pp
565
- 566 Cook, K. H., 1999: Generation of the African easterly jet and its role in determining West
567 African precipitation. *J. Climate*, 12, 1165–1184, doi:10.1175/1520-
568 0442(1999)012<1165:GOTAEJ>2.0.CO;2.
569



- 570 Dee et al (2011) The ERA-Interim reanalysis: configuration and performance of the data
571 assimilation system. *Quat J R Meteorol Soc* 137:553–597. doi:10.1002/qj.828
572
- 573 Diallo I, Sylla MB, Camara M, Gaye AT. 2012. Interannual variability of rainfall and
574 circulation features over the Sahel based on multiple regional climate models simulations.
575 *Theor. Appl. Climatol.* DOI:10.1007/s00704-012-0791-y.
576
- 577 Diallo I, Sylla MB, Camara M, Gaye AT (2013) Interannual variability of rainfall over the Sahel
578 based on multiple regional climate models simulations. *Theor Appl Climatol.*
579 doi:10.1007/s00704-012-0791-y
580
- 581 Dickinson, R., A. Henderson-Sellers, and P. Kennedy. 1993. “Biosphere-Atmosphere Transfer
582 Scheme (BATS) Version 1eas Coupled to the NCAR Community Climate Model.” NCAR
583 Technical Note, NCAR/TN-387+ STR, 72 pp.
584
- 585 Diedhiou, A., Janicot, S., Viltard, A., De Felice, P., & Laurent, H. (1999). Easterly wave
586 regimes and associated convection over West Africa and tropical Atlantic: Results from the
587 NCEP/NCAR and ECMWF reanalyses. *Climate Dynamics*, 15(11), 795-822.
588
- 589 Djiotang Tchotchou LA, Mkankam Kanga F. 2010. Sensitivity of the simulated African
590 monsoon of summers 1993 and 1999 to convective parameterization schemes in RegCM3.
591 *Theor. Appl. Climatol.* 100: 207–220.
592
- 593 Emanuel, K. 1991. “A Scheme for Representing Cumulus Convection in Large-Scale Models.”
594 *Journal of the Atmospheric Sciences* 48: 2313-2329.
595
- 596 Emanuel KA, Zivkovic-Rothman M (1999) Development and evaluation of a convection
597 scheme for use in climate models. *J Atmos Sci* 56:1766–1782
598
- 599 Fritsch JM, Chappell CF (1980) Numerical prediction of convectively driven mesoscale
600 pressure systems. Part I: Convective parameterization. *J Atmos Sci* 37: 722–1733
601



- 602 Gao, X., Y. Shi, D. Zhang, J. Wu, F. Giorgi, Z. Ji, and Y. Wang. 2012. “Uncertainties in
603 Monsoon Precipitation Projections over China: Results from Two High-Resolution RCM
604 Simulations.” *Climate Research* 52: 213–226.
605
- 606 Gao Xue-Jie, Ying SHI, Filippo GIORGI, (2016). Comparison of convective parameterizations
607 in RegCM4 experiments over China with CLM as the land surface model. *Atmospheric and
608 Oceanic Science Letters*, 9:4, 246-254, DOI: 10.1080/16742834.2016.1172938
609
- 610 Gbobaniyi E, Sarr A, Sylla MB, Diallo I, Lennard C, Diedhiou A et al (2013) Climatology,
611 annual cycle and interannual variability of precipitation and temperature in CORDEX regional
612 climate models simulation over West Africa. *Inter J Climatol*. doi:10.1002/joc.3834
613
- 614 Giorgi F, Coppola E, Solmon F, Mariotti L, Sylla MB, Bi X, Elguindi N, Diro GT, Nair V,
615 Giuliani G, Cozzini S, Guettler I, O’Brien T, Tawfik A, Shalaby A, Zaakey AS, Steiner A,
616 Stordal F, Sloan L, Brankovic C. 2012. RegCM4: model description and preliminary tests over
617 multiple CORDEX domains. *Climate Res.* 52: 7–29, DOI:v10.3354/cr01018.
618
- 619 Grell G, Dudhia J, Stauffer DR (1994) A description of the fifth generation Penn State/NCAR
620 Mesoscale Model (MM5). National Center for Atmospheric Research Tech Note NCAR/TN-
621 398+STR, NCAR, Boulder, CO
622
- 623 Grell, G. 1993. “Prognostic Evaluation of Assumptions Used by Cumulus Parameterizations.”
624 *Monthly Weather Review* 121: 764-787.
625
- 626 Halder S., Dirmeyer P. and K. Saha, 2015. “Sensitivity of the Mean and Variability of Indian
627 Summer Monsoon to Land Surface Schemes in RegCM4: Understanding Coupled Land-
628 Atmosphere Feedbacks.” *Journal of Geophysical Research* 120:9437–9458
629
- 630 Harris I, Jones PD, Osborn TJ, Lister DH (2013) Updated high-resolution grids of monthly
631 climatic observations. *Int J Climatol*. doi:10.1002/joc.3711
632
- 633 Holtslag A, De Bruijn E, Pan H-L (1990) A high resolution air mass transformation model for
634 short-range weather forecasting. *Mon Wea Rev* 118: 1561–1575
635



- 636 Huffman GJ, Adler RF, Bolvin DT, Gu G, Nelkin EJ, Bowman KP, Hong Y, Stocker EF, Wolff
637 DB (2007) The TRMM multisatellite precipitation analysis: quasi-global, multi-year,
638 combined-sensor precipitation estimates at fine scale. *J Hydrometeorol* 8:38–55
639
- 640 Hourdin F, Musat I, Guichard F, Ruti PM, Favot F, Filiberti MA, Pham M, Grandpeix JY,
641 Polcher J, Marquet P, Boone A, Lafore JP, Redelsperger JL, Dell’aquila A, Doval TL, Traore
642 AK, Gall’ee H. 2010. AMMA-model intercomparison project. *Bull. Am. Meteorol.Soc.* 91(1):
643 95–104.
644
- 645 Im, E., J. Ahn, A. Remedio, and W.-T. Kwon. 2008. “Sensitivity of the Regional Climate of
646 East/Southeast Asia to Convective Parameterizations in the RegCM3 Modelling System. Part
647 1: Focus on the Korean Peninsula.” *International Journal of Climatology* 28: 1861–1877.
648
- 649 IPCC. 2007. *Climate Change 2007: The Physical Science Basis. Contribution of Working group*
650 *I to the Fourth Assessment Report of the Intergovernmental Panel on Climate Change*, Solomon
651 S, Qin D, Manning M, Chen Z, Marquis M, Averyth KB, Tignor M, Miller HL (eds). Cambridge
652 University Press: Cambridge, UK, 996 pp.
653
- 654 Janicot S, Caniaux G, Chauvin F, de Coetlogon G, Fontaine B, Hall N, Killadis G, Lafore J-P,
655 Lavaysse C, Lavender SL, Leroux S, Marteau R, Mounier F, Philippon N, Roehrig R, Sultan
656 B, Taylor CM (2011) Intraseasonal variability of the West African monsoon. *Atmos Sci Lett*
657 12:58–66. doi:10.1002/asl.280
658
- 659 Kain, J. S., and J. M. Fritsch, 1990: A one-dimensional entraining/detraining plume model and
660 its application in convective parameterization. *J. Atmos. Sci.*, 47, 2784–2802.
661
- 662 Kain J. S, 2004. The Kain–Fritsch Convective Parameterization: An Update. *Journal of Applied*
663 *Meteorology*. Vol. 43, Issue 1, pp.170-181.
664
- 665 Kamga Foamouhoue A, Buscarlet ´ E. 2006. Simulation du climat de l’Afrique de l’Ouest à
666 l’aide d’un modèle climatique régional: validation sur la période 1961–1990.
667



- 668 Komkoua Mbienda A. J., Tchawoua C., Vondou D. A., Choumbou P., Kenfack Sadem C., and
669 Dey S, 2016. Sensitivity experiments of RegCM4 simulations to different convective schemes
670 over Central Africa. *Int. J. Climatol.* DOI: 10.1002/joc.4707
671
- 672 Kiehl JT Hack JJ, Bonan GB, Boville BA, Briegleb BP, Williamson DL, Rasch PJ (1996)
673 Description of the NCAR Community Climate Model (CCM3). Technical Note NCAR/TN—
674 420+STR, p 152
675
- 676 Konare A, Zakey AS, Solmon F, Giorgi F, Rauscher S, Ibrah S, Bi X. 2008. A regional climate
677 modeling study of the effect of desert dust on the West African monsoon. *J. Geophys. Res.*
678 113(D12): D12206.
679
- 680 Meinke I, Roads J, Kanamitsu M. 2007. Evaluation of RSM-simulated precipitation during
681 CEOP. *J. Meteorol. Soc. Jpn.* 85A: 145–166.
682
- 683 Mohr, K. I., and C. D. Thorncroft, 2006: Intense convective systems in West Africa and their
684 relationship to the African easterly jet. *Quart. J. Roy. Meteor. Soc.*, 132, 163–176,
685 doi:10.1256/qj.05.55.
686
- 687 N'Datchoh E. T. , Diallo I., Konaré A., Silué S., Ogunjobi K.O., Diedhiou A., Doumbia M.
688 (2017) Dust induced changes on the West African summer monsoon features. *Int J Climatol*,
689 DOI: 10.1002/joc.5187.
690
- 691 Nicholson SE (2013) The West African Sahel: a review of recent studies on the rainfall regime
692 and its interannual variability. *Meteorology*. Volume 2013, Article ID 453521, 32 pages.
693 doi:10.1155/2013/453521
694
- 695 Nikulin G, Jones C, Samuelsson P, Giorgi F, Asrar G, Bu'chner M, Cerezo-Mota R, Christensen
696 OB, De'que' M, Fernandez J, Hansler A, van Meijgaard E, Sylla MB, Sushama L (2012)
697 Precipitation climatology in an ensemble of CORDEX-Africa regional climate simulations. *J*
698 *Clim* 6057–6078. doi:10.1175/JCLI-D-11-00375.1
699



700 Lawrence, D. M., et al.,(2011), Parameterization improvements and functional and structural
701 advances in version 4 of the Community Land Model, *J. Adv. Model. Earth Syst.*, 3, M03001,
702 doi:10.1029/2011MS000045.

703

704 Legates DR, Willmott CJ (1990) Mean seasonal and spatial variability in gauge-corrected,
705 global precipitation. *Int J Climatol.*, 10:111–127

706

707 Leung, L., S. Zhong, Y. Qian, and Y. Liu. 2004. “Evaluation of Regional Climate Simulations
708 of the 1998 and 1999 East Asian Summer Monsoon Using the GAME/HUBEX Observational
709

710 Loveland TR, Reed BC, Brown JF, Ohlen DO, Zhu J, Yang L, Merchant JW (2000)
711 Development of a global land cover characteristics database and IGBP DISCover from 1-km
712 AVHRR Data. *Int J Remote Sensing* 21: 1303–1330

713

714 Martínez-Castro, D., da Rocha, R. P., Bezanilla-Morlot, A., Alvarez-Escudero, L., Reyes-
715 Fernández, J. P., Silva-Vidal, Y., & Arritt, R. W. (2006). Sensitivity studies of the RegCM3
716 simulation of summer precipitation, temperature and local wind field in the Caribbean Region.
717 *Theoretical and Applied Climatology*, 86(1-4), 5-22. DOI 10.1007/s00704-005-0201-9.

718

719 Oleson, K., G. Niu, Z. Yang, D. Lawrence, P. Thornton, P. Lawrence, et al.,2008.
720 “Improvements to the Community Land Model and Their Impact on the Hydrological Cycle.”
721 *Journal of Geophysical Research* 113: G01021. doi: <http://dx.doi.org/10.1029/2007JG000563>.

722

723 Oleson KW, Lawrence DM, Bonan GB et al (2013) Technical description of version 4.5 of the
724 Community Land Model (CLM). NCAR technical note NCAR/TN-503 + STR. National Center
725 for Atmospheric Research, Boulder

726

727 Paeth H. and Hense A., “SST versus climate change signals in West African rainfall: 20th-
728 century variations and future projections,” *Climatic Change*, vol. 65,no. 1-2, pp. 179–208, 2004.

729

730 Paeth H., Girmes R., Menz G., and Hense A., “Improving seasonal forecasting in the low
731 latitudes,” *Monthly Weather Review*, vol. 134, no. 7, pp. 1859–1879, 2006.

732



- 733 Paeth H, Hall NM, Gaertner MA, Alonso MD, Moumouni S, Polcher J, Ruti PM, Fink AH,
734 Gosset M, Lebel T, Gaye AT, Rowell DP, Moufouma-Okia W, Jacob D, Rockel B, Giorgi F,
735 Rummukainen M. 2011. Progress in regional downscaling of West African precipitation.
736 Atmos. Sci. Lett. 12(1): 75–82.
737
- 738 Pal JS, Small EE, Elthair EA (2000) Simulation of regionalscale water and energy budgets:
739 representation of subgrid cloud and precipitation processes within RegCM. J Geophys Res 105:
740 29579–29594
741
- 742 Pal JS, Giorgi F, Bi X, Elguindi N, Solomon F, Gao X, Francisco R, Zakey A, Winter J, Ashfaq
743 M, Syed F, Bell JL, Diffanbaugh NS, Kamacharya J, Konare A, Martinez D, da Rocha RP,
744 Sloan LC, Steiner A (2007) The ICTP RegCM3 and RegCNET: regional climate modeling for
745 the developing world. Bull Amer Meteor Soc 88:1395–1409
746
- 747 Reynolds RW, Smith TM (1994) Improved global sea surface temperature analysis using
748 optimum interpolation. J Climate 7: 929–948
749
- 750 Simmons AS, Uppala DD, Kobayashi S (2007) ERA-interim: new ECMWF reanalysis products
751 from 1989 onwards. ECMWF Newsl 110:29–35
752
- 753 Singh AP, Singh RP, Raju PVS, Bhatla R. 2011. Comparison of three different cumulus
754 parameterization schemes on Indian summer monsoon circulation. Int. J. Ocean Clim. Syst.
755 2(1): 27–43
756
- 757 Smith SD (1988) Coefficients for sea surface wind stress, heat flux, and wind profiles as a
758 function of wind speed and temperature. J Geophys Res 93: 15467–15472
759
- 760 Soden BJ, Held IM. 2006. An assessment of climate feedbacks in coupled ocean–atmosphere
761 model. J. Clim. 19: 3354–3360.
762
- 763 Solmon F, Giorgi F, Liousse C (2006) Aerosol modeling for regional climate studies:
764 application to anthropogenic particles and evaluation over a European/African domain. Tellus
765 Ser B Chem Phys Meteorol 58:51–72
766



- 767 Srinivas CV, Hariprasad D, Rao DVB, Anjaneyulu Y, Baskaran R, Venkataraman B. 2013.
768 Simulation of the Indian summer monsoon regional climate using advanced research WRF
769 model. *Int. J. Climatol.* 33: 1195–1210.
770
- 771 Steiner, A., J. Pal, S. Rauscher, J. Bell, N. Diffenbaugh, A. Boone, L. Sloan, et al., 2009. “Land
772 Surface Coupling in Regional Climate Simulations of the West African Monsoon.” *Climate*
773 *Dynamics* 33: 869–892.
774
- 775 Sultan B, Janicot S. 2000. Abrupt shift of the ITCZ over West Africa and intra-seasonal
776 variability. *Geophysical Research Letters* 27:3353–3356.
777
- 778 Sultan, B., Janicot, S., & Diedhiou, A. (2003). The West African monsoon dynamics. Part I:
779 Documentation of intraseasonal variability. *Journal of Climate*, 16(21), 3389-3406.
780
- 781 Sultan B, Janicot S. 2003. The West African monsoon dynamics. Part II: The “preonset” and
782 “onset” of the summer monsoon. *J. Climate* 16(21): 3407–3427.
783
- 784 Sundqvist HE, Berge E, Kristjansson JE (1989) The effects of domain choice on summer
785 precipitation simulation and sensitivity in a regional climate model. *J Climate* 11: 2698–2712
786
- 787 Sylla MB, Gaye AT, Pal JS, Jenkins GS, Bi XQ. 2009. High resolution simulations of West
788 Africa climate using Regional Climate Model (RegCM3) with different lateral boundary
789 conditions. *Theor. Appl. Climatol.* 98(3–4): 293–314, DOI: 10.1007/s00704-009-0110-4.
790
- 791 Sylla MB, Giorgi F, Ruti PM, Calmanti S, Dell’Aquila A. 2011. The impact of deep convection
792 on the West African summer monsoon climate: a regional climate model sensitivity study. *Q.*
793 *J. Roy. Meteorol. Soc.* 137: 1417–1430, DOI: 10.1002/qj.853.
794
- 795 Sylla MB, Giorgi F, Stordal F. 2012. Large-scale origins of rainfall and temperature bias in
796 high resolution simulations over Southern Africa. *Climate Res.* 52: 193–211, DOI:
797 10.3354/cr01044.
798



- 799 Sylla MB, Giorgi F, Coppola E, Mariotti L (2013a) Uncertainties in daily rainfall over Africa:
800 assessment of observation products and evaluation of a regional climate model simulation. Int
801 J Climatol. doi:10.1002/joc.3551
802
- 803 Sylla MB, Diallo I, Pal JS., 2013b. West African monsoon in state of the art regional climate
804 models. In Climate Variability Regional and Thematic Patterns, Tarhule A (ed). ISBN: 980-
805 953-307-816-3.
806
- 807 Tadross MA, Gutowski WJ Jr, Hewitson BC, Jack C, New M. 2006. MM5 simulations of
808 interannual change and the diurnal cycle of
809 southern African regional climate. Theor. Appl. Climatol. 86(1–4): 63–80.
810
- 811 Thorncroft CD, Blackburn M (1999) Maintenance of the African easterly jet. Q J R Meteorol
812 Soc 125:763–786
813
- 814 Tiedtke, M. 1989. “A Comprehensive Mass Flux Scheme for Cumulus Parameterization in
815 Large-scale Models.” Monthly Weather Review 117: 1779–1800.
816
- 817 Uppala S, Dee D, Kobayashi S, Berrisford P, Simmons A (2008) Towards a climate data
818 assimilation system: status update of ERA-interim. ECMWF Newsl 115:12–18
819
- 820 Wang, G., M. Yu, J. S. Pal, R. Mei, G. B. Bonan, S. Levis, and P. E. Thornton (2016), On the
821 development of a coupled regional climate vegetation model RCM-CLM-CN-DV and its
822 validation its tropical Africa, *Clim. Dyn.*, 46, 515–539.
823
- 824 Xue Y, De Sales F, Lau KMW, Bonne A, Feng J, Dirmeyer P, Guo Z, Kim KM, Kitoh A,
825 Kumar V, Pocard-Leclercq I, Mahowald N, Moufouma-Okia W, Pegion P, Rowell DP,
826 Schemm J, Schulbert S, Sealy A, Thiaw WM, Vintzileos A, Williams SF, Wu ML (2010)
827 Intercomparison of West African Monsoon and its variability in the West African Monsoon
828 Modelling Evaluation Project (WAMME) first model Intercomparison experiment. *Clim Dyn.*
829 doi:10.1007/s00382-010-0778-2
830
- 831 Zakey AS, Solmon F, Giorgi F (2006) Implementation and testing of a desert dust module in a
832 regional climate model. *Atmos Chem Phys*, 6:4687–4704



833

834 Zaroug MAH, Sylla MB, Giorgi F, Eltahir EAB, Aggarwal PK. 2012. A sensitivity study on
835 the role of the Swamps of Southern Sudan in the summer climate of North Africa using a
836 regional climate model. *Theor. Appl. Climatol.* DOI: 10.1007/s00704-012-0751-6.

837

838 Zeng X, Zhao M, Dickinson RE (1998) Intercomparison of bulk aerodynamic algorithms for
839 the computation of sea surface fluxes using TOGA COARE and TAO DATA. *J Climate* 11:
840 2628–2644

841

842

843

844

845

846

847

848

849

850

851

852



853

854

855

856

857

858

859

860

861

862

863

864

865

866

867

868

869

870

871

872

873

874

875

876

877

878

879

880

881

882

883

884

885

886

	Guinea Coast		Sahel Central		West Sahel		West Africa	
	RMSD (°C)	PCC	RMSD (°C)	PCC	RMSD (°C)	PCC	RMSD (°C)	PCC
UDEL	0.613	0.749	0.475	0.974	0.424	0.981	0.695	0.981
Mix1	1.605	0.768	0.737	0.961	0.720	0.987	1.218	0.978
Emanuel	1.294	0.772	0.673	0.954	0.589	0.986	1.068	0.979
Grell	2.657	0.728	1.406	0.920	1.994	0.985	2.171	0.973
Tiedtke	1.534	0.758	1.360	0.938	0.717	0.982	1.355	0.938
Mix2	1.993	0.781	1.682	0.884	1.568	0.978	1.715	0.964

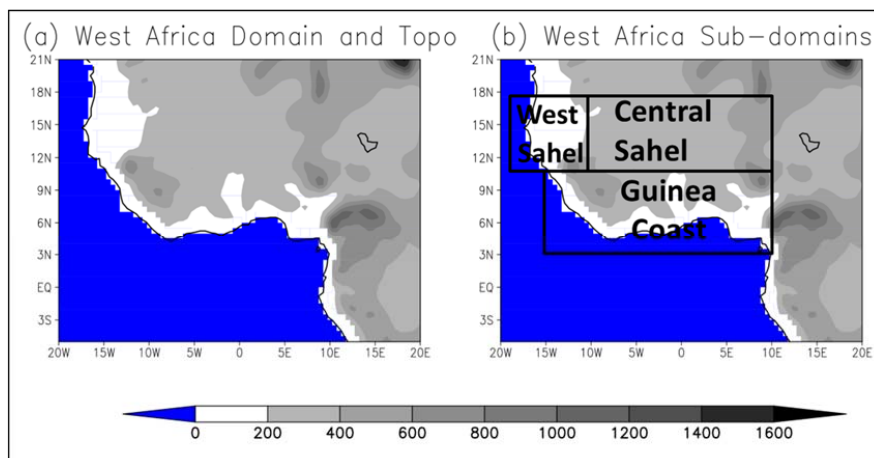
Table 1: pattern correlation coefficient (PCC) and root mean square difference (RMSD) for JJAS 2m-temperature for model simulations and observation (UDEL) with respect to CRU over different sub-regions.

	Guinea Coast	Sahel Central	West Sahel	West Africa	PCC
	Mean Bias (%)	Mean Bias (%)	Mean Bias (%)	Mean Bias (%)	
TRMM	-0.86	-5.26	3.48	0.82	0.964
Mix1	-18.31	-39.78	-15.36	-22.25	0.721
Emanuel	-27.22	-42.30	-33.63	-25.58	0.810
Grell	-49.69	-57.21	-51.92	-34.07	0.663
Tiedtke	-48.71	-77.14	-56.67	-65.08	0.613
Mix2	-54.43	-50.55	-55.42	-47.66	0.897

Table 2: mean bias (MB) and the pattern correlation coefficient (PCC) for JJAS precipitation for model simulations and observation (TRMM) with respect to GPCP. The PCC is calculated only for the West African region.



887
888
889

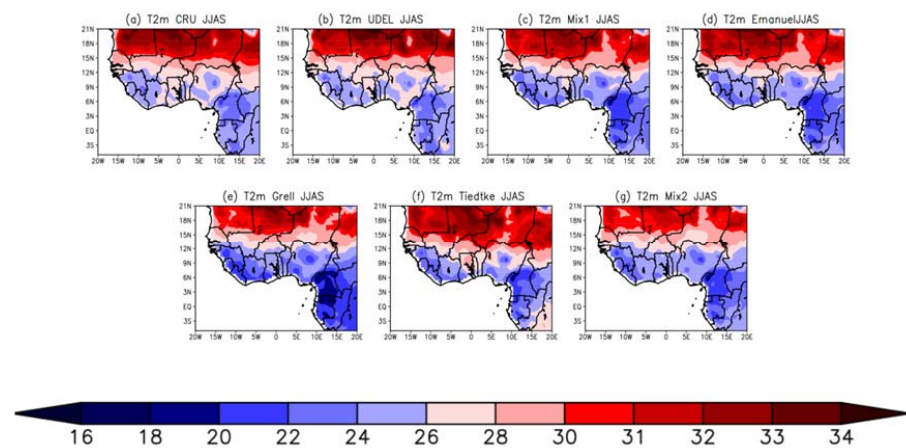


890
891
892
893
894
895
896
897
898
899
900
901
902
903
904
905
906
907
908
909
910

Figure 1: Domain, topography and sub-regions.



911
912
913



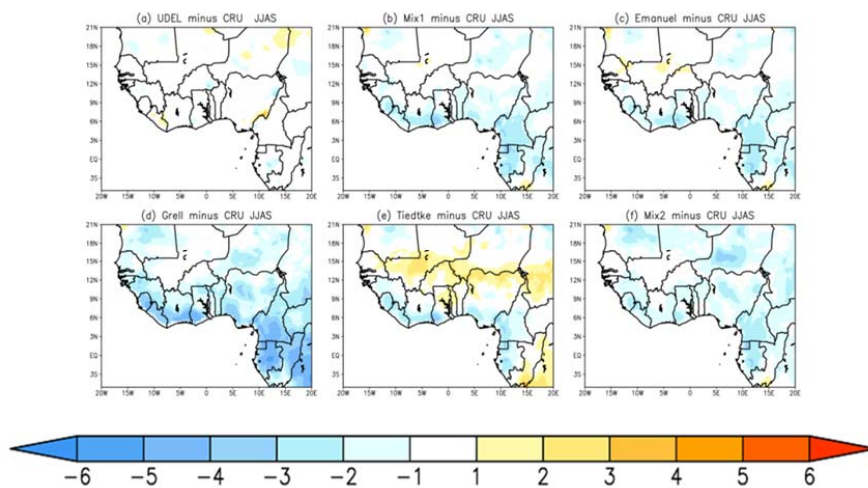
914
915
916
917
918
919
920
921
922
923
924
925
926
927
928
929
930
931
932
933
934

Figure 2: Averaged 2003–2004 JJAS 2m-temperature (in °C) from: (a) CRU, (b) UDEL, (c) Mix1, (d) Emanuel, (e) Grell, (f) Tiedtke and (g) Mix2.



935

936



937

938

939 **Figure 3:** JJAS 2m-temperature bias (in °C) with respect to CRU from: (a) UDEL, (b)

940 Mix1, (c) Emanuel, (d) Grell, (e) Tiedtke and (f) Mix2.

941

942

943

944

945



946

947

948

949

950

951

952

953

954

955

956

957

958

959

960

961

962

963

964

965 **Figure 4:** PDF distributions (%) of temperature bias in JJAS over Guinea, Central Sahel,
966 West Sahel and West Africa, derived from the model simulations using different convection
967 schemes (land only; units: °C).

968

969

970

971

972

973

974

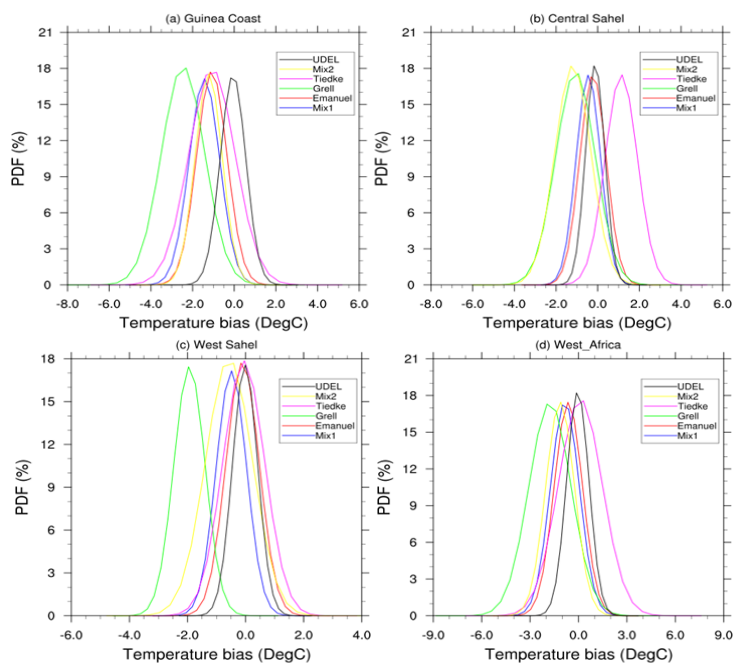
975

976

977

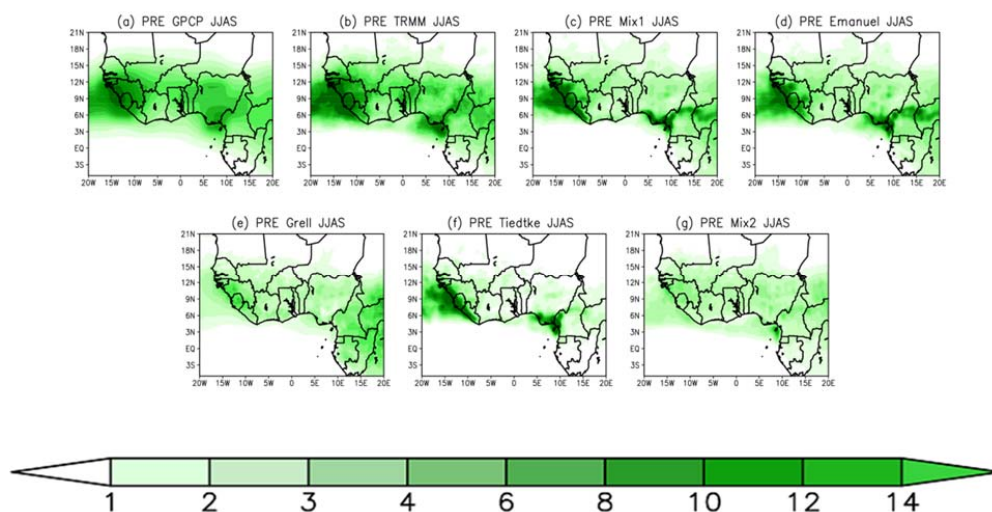
978

979





980
981
982



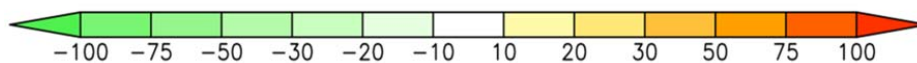
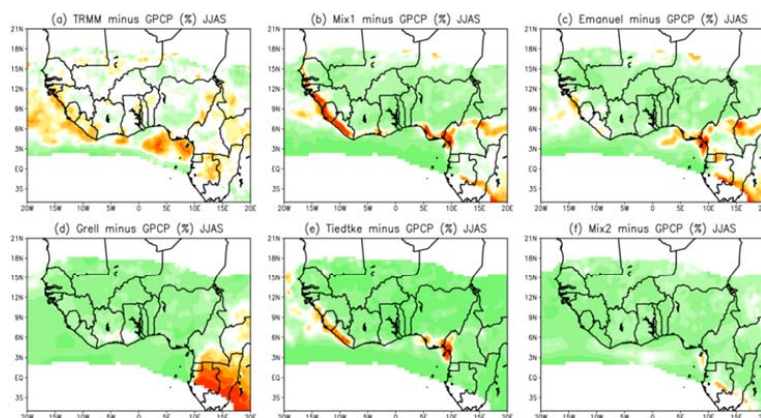
983
984
985
986
987
988
989
990
991
992
993
994
995
996
997
998
999
1000
1001

Figure 5: Averaged 2003–2004 JJAS precipitation (in mm/day) from: (a) GPCP, (b) TRMM, (c) Mix1, (d) Emanuel, (e) Grell, (f) Tiedtke and (g) Mix2.



1002

1003



1004

1005

1006 **Figure 6:** JJAS precipitation bias (in %) with respect to GPCP from : (a) TRMM, (b)

1007 Mix1, (c) Emanuel, (d) Grell, (e) Tiedtke and (f) Mix2.

1008

1009

1010

1011

1012

1013

1014

1015

1016

1017

1018

1019

1020

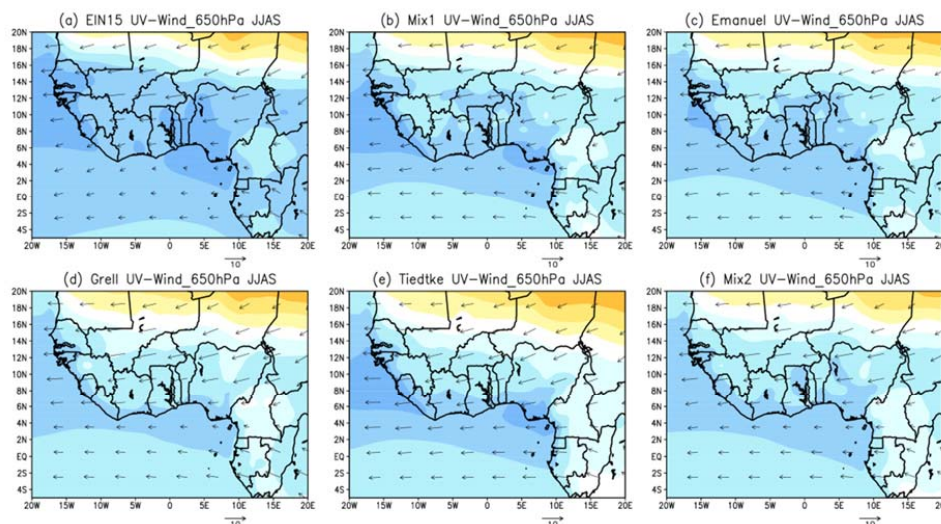
1021

1022

1023



1024
1025
1026



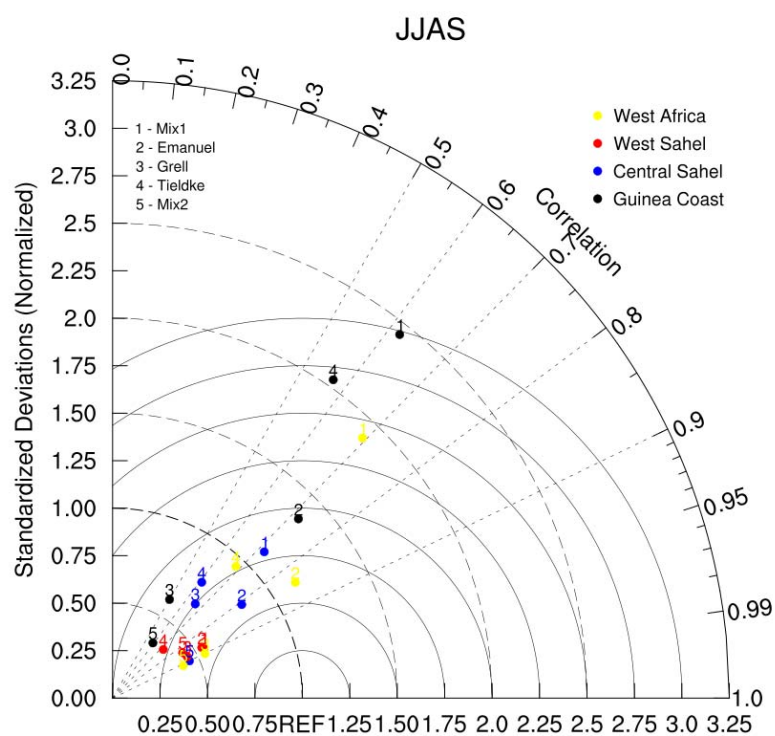
1027
1028
1029
1030
1031
1032
1033
1034
1035
1036
1037
1038
1039
1040
1041
1042
1043
1044

Figure 7: The (a) observed and (b–f) simulated vertically mean midlevel (850–300 hPa) integrated specific humidity (shaded) superimposed at zonal winds in JJAS at 650 hPa from (a) ERA-Interim, (b) Mix1 (c) Emanuel, (d) Grell (e) Tiedtke and (f) Mix2. Arrows are in m/s and specific humidity is expressed in 10^{-3} kg/kg.



1045

1046



1047

1048

1049

1050

1051

1052

1053

1054

1055

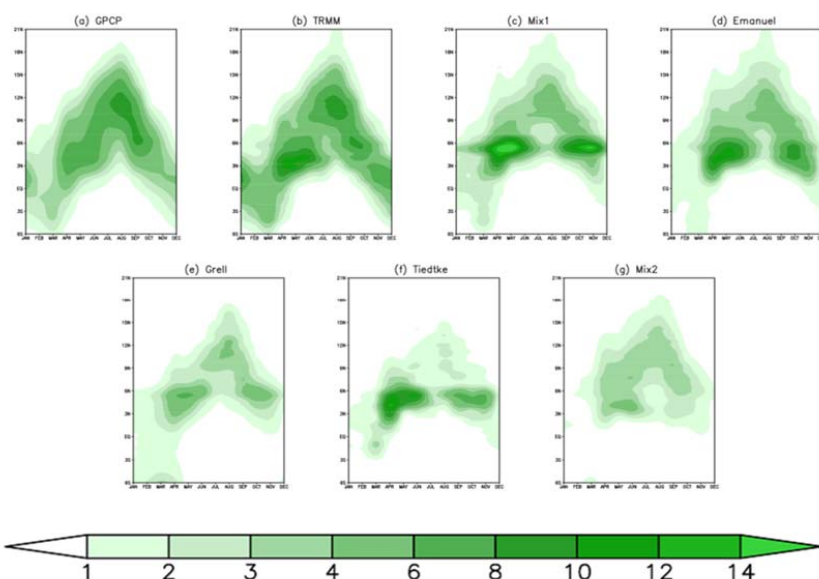
1056

Figure 8: Taylor diagram showing the pattern correlation and the standard deviation (Normalized) of precipitation with respect to GPCP from: Mix1, Emanuel, Grell, Tiedtke and Mix2 over Guinea Coast, Central Sahel, West Sahel and West Africa.



1057

1058



1059

1060

1061

Figure 9: Hovmoller diagram of monthly precipitation (mm/day) averaged between 10°W and 10°E and for the period 2003-2004 for (a) GPCP, (b) TRMM, (c) Mix1, (d) Emanuel, (e) Grell, (f) Tiedtke and (g) Mix2.

1063

1064

1065

1066

1067

1068

1069

1070

1071

1072

1073

1074

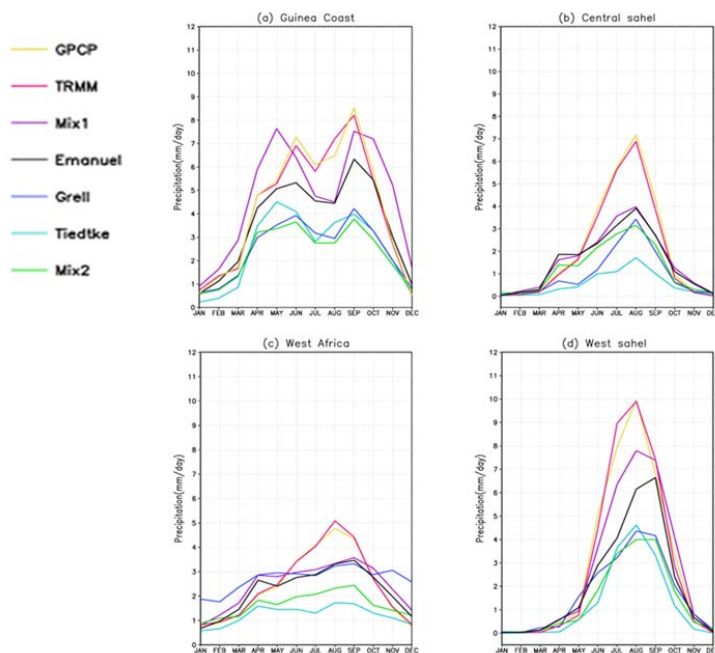
1075

1076

1077



1078
1079
1080

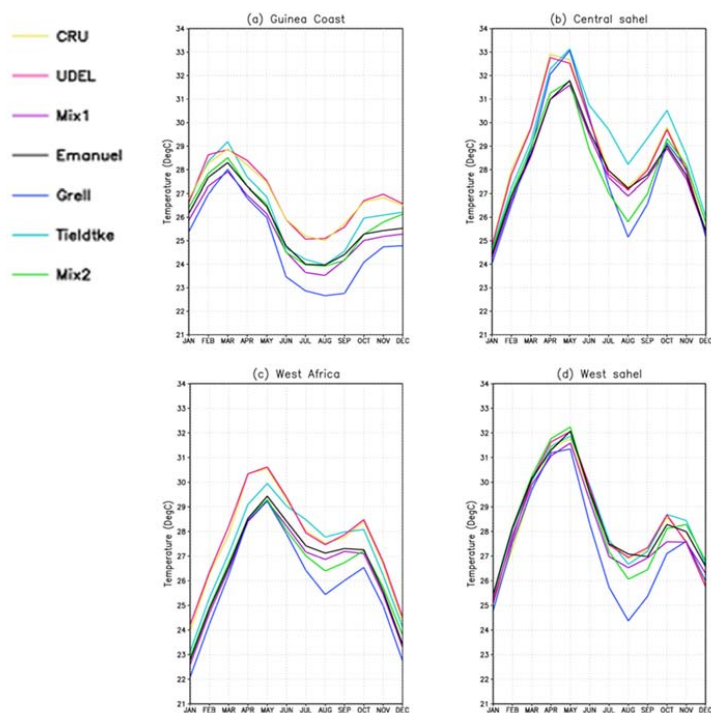


1081
1082
1083
1084
1085
1086
1087
1088
1089
1090
1091
1092
1093
1094
1095
1096
1097

Figure 10: Annual cycle of monthly precipitation ($\text{mm}\cdot\text{day}^{-1}$) averaged over, (a) the Guinea Coast West and (b) Central Sahel, (c) West Africa and (d) West Sahel for the period 2003–2004.



1098
1099
1100

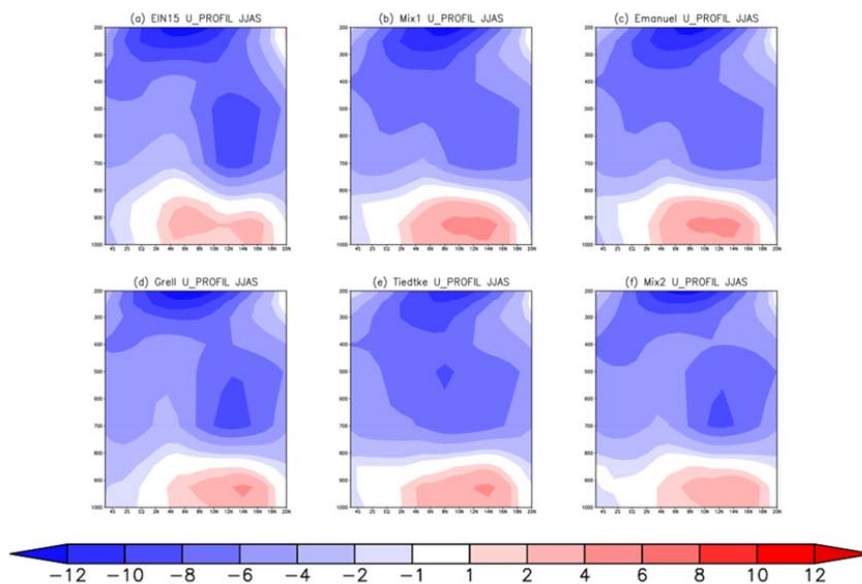


1101
1102
1103
1104
1105
1106
1107
1108
1109
1110
1111
1112
1113
1114
1115

Figure 11: Annual cycle of 2m-Temperature (°C) averaged over, (a) the Guinea Coast, (b) Central Sahel, (c) West Africa and (d) West Sahel for the period 2003–2004.



1116
1117
1118
1119



1120
1121
1122
1123
1124
1125
1126

Figure 12: Vertical cross section of the JJAS mean zonal wind (in m/s) averaged between 10°W–10°E from: (a) ERA-Interim (b) Mix1, (c) Emanuel, (d) Grell, (e) Tiedtke and (f) Mix2. The mean is calculated using the 2003–2004 period.